Journal of Molecular Spectroscopy **214,** 202–215 (2002)
doi:10.1006/jmsp.2002.8588

Spectroscopy of $\Sigma 0_0 \rightarrow \Pi 1_0$ Vibrational–Tunneling–Rotational Band in $Rg \cdot ND_3$ (Rg = Ne, Ar, Kr)

Dmitry G. Melnik,* Terry A. Miller,* and Frank C. De Lucia†

*Department of Chemistry, The Ohio State University, 120 West 18th Avenue, Columbus, Ohio 43210; and †Department of Physics, 174 West 18th Avenue, Columbus, Ohio 43210

E-mail: tamiller+@osu.edu, fcd@mps.ohio-state.edu

Received February 22, 2002; in revised form April 12, 2002

A number of vibrational–tunneling–rotational (VTR) transitions in the range of 195–298 GHz belonging to the $\Sigma 0_0 \rightarrow \Pi 1_0$ hindered rotation band in $Rg \cdot ND_3$ (Rg = Ne, Kr) complexes are observed in absorption in a free supersonic jet, using the pulsed fast scan submillimeter-wave spectroscopic technique (FASSST). The data obtained in this experiment, combined with previously obtained data on the $Ar \cdot ND_3$ complex, were used to construct a qualitative model describing the inversion–tunneling motion in the lowest states of the $Rg \cdot ND_3$ complexes.

I. INTRODUCTION

Van der Waals complexes are attractive physical systems for study to provide information about weak intermolecular interactions that are relevant to the study of chemical kinetics, solution dynamics, and other fields. Complexes that contain rare gas (Rg) atoms are of particular interest because Rg atoms may be regarded as structureless probes of the "shape" of the intermolecular potential surface.

The energy level diagram of the lowest states of the $Rg \cdot ND_3$ complex correlating to the $j = 0$, 1 and $k = 0$ of the ammonia monomer (*1*) is shown in Fig. 1. In perdeuterated ammonia the $k = 0$ levels are split into two inversion components corresponding to symmetric and antisymmetric inversion states, denoted in Fig. 1 by + and − respectively. These states also correspond to different nuclear spin functions that transform as A_1' and A_2' representations of the PI group isomorphous to D_{3h} (*1*). Following the notation of Schmuttenmaer *et al.* (*2, 3*), the energy levels of the complex are correlated with those of the free ammonia molecule and designated as Σj_k, Πj_k, etc., where Σ corresponds to $\Omega = 0$ and Π to $\Omega = 1$. Ω denotes the projection of the complex total angular momentum $\boldsymbol{J}$ on the van der Waals bond $\boldsymbol{R}_{vdW}$, defined as the line connecting the centers of mass of the two moieties, with the j and k quantum numbers correlating with the corresponding states of free ND_3. The Coriolis interaction between the $\Pi 1_0$ and $\Sigma 1_0$ states lifts the Ω-degeneracy of the $\Pi 1_0$ state and gives rise to the splitting into two states denoted as Π^+ and Π^- in Fig. 1c.

Of all the van der Waals complexes previously studied, $Ar \cdot NH_3$ (*4–11, 3, 12, 2*) and $Ar \cdot ND_3$ (*13, 1*) are the simplest molecules exhibiting inversion–tunneling motion. The first studies of the $Ar \cdot NH_3$ complex were done in the microwave region (*4, 5*). The experimental results led to the conclusion that the ammonia monomer undergoes both nearly free rotation and only slightly perturbed inversion. Later, submillimeter and far infrared studies of the bending modes correlating to the $k = 0$ (*9*) and $|k| = 1$ (*8*) were done. The latter studies showed that due to the asymmetry of the inversion potential in the states with both nonzero $|k|$ and Ω quantum numbers, the inversion splitting is significantly quenched, while for $\Sigma 1_0$ state ($\Omega = 0$) the inversion remains only slightly perturbed.

A number of *ab initio* calculations (*6, 7, 11, 10*) of the potential energy surface (PES) have been done for $Ar \cdot NH_3$. The results suggest that the PES minimum is about $D_e = 115$ to 134 cm^{-1} (*11, 7, 6*), and the corresponding dissociation energy D_0 is about 82 cm^{-1} (*11*). Van Bladel *et al.* (*11, 10*) have predicted the rovibronic level pattern and generated a theoretical spectrum of the $Ar \cdot NH_3$ complex. Schmuttenmaer *et al.* (*3*) experimentally studied the van der Waals Σ and Π bends and Σ–Σ stretch bands in the manifold correlating to $k = 0$ stacks and derived the potential surface from the spectroscopic data. They have also derived from the quadrupole analysis the structure of the molecule, averaged over large-amplitude motions, and showed that within experimental error, the quadrupole coupling constant of ammonia is unaffected by complexation. Grushow *et al.* (*14*) and Schmuttenmaer *et al.* (*12*) extended the experimental and theoretical studies to higher lying (correlating to up to $j = 2$) states.

However, the inversion motion in the states with $k = 0$ in $Ar \cdot NH_3$ could not be directly observed experimentally since one of the inversion states in the $k = 0$ stacks of NH_3 is Pauli forbidden. This makes $Ar \cdot ND_3$ a logical choice of a test system, since both states are allowed in ND_3. In addition, the inversion splitting in the ground vibrational state of ND_3 is about 11 times smaller

0022-2852/02 $35.00

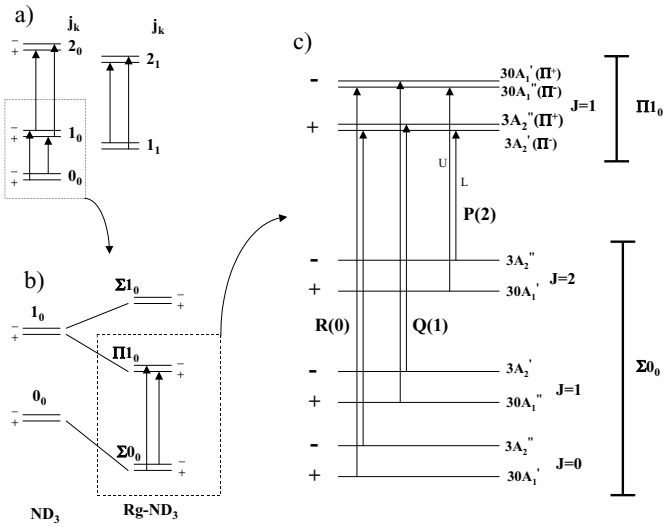

FIG. 1. Energy level and transition diagram for ND_3 and Rg · ND_3. (a) Energy levels in monomer, (b) correlation between the energy levels in ND_3 and Rg · ND_3, (c) Π-bend transition in Rg · ND_3. Energy levels include overall rotation of the complex. The full rovibrational–inversional symmetry (A_1', etc.) is indicated, with the indicating numbers preceding the nuclear spin statistical weight. The + and − signs label inversion levels. In case of Rg · ND_3 these signs are not rigorous quantum numbers but indicate correlation with the corresponding symmetry components in monomer. L and U label transitions corresponding to the lower and the upper frequency components of the band, respectively.

than that in NH_3 putting the van der Waals motions and inversion in different parts of the frequency scale allowing for simpler modeling. Based on the predictions of Schmuttenmaer *et al.* (*2*) we have previously studied Π-bend excitation ($\Sigma 0_0 \rightarrow \Pi 1_0$ band) in Ar · ND_3 (*1*). We found that the inversion splitting is slightly perturbed, as in the case of $\Sigma 1_0$ of Ar · NH_3 (*8*).

Recently, a series of experiments on Rg · ND_3 complexes were done by Wijngaarden and Jager (*13, 15, 16*) who reported the rotational spectra within the ground $\Sigma 0_0$ states of the neon, argon, and krypton complexes, which were obtained in microwave FT experiments. This and the present data set are highly complementary.

The limited set of the experimental data from the narrow accessible spectral range did not allow us to develop a model describing inversion–tunneling motion in any detail. In the present work we have extended our studies to the corresponding transitions in Ne · ND_3 and Kr · ND_3 with the aim of learning more about bonding in the lowest states of Rg · ND_3 complexes and to develop a qualitative model of the interaction.

II. EXPERIMENTAL

The experimental data were acquired using the pulsed jet FASSST spectrometer described elsewhere (*1*) and only a brief description is given here. The rapidly (100–120 GHz/s) scanned radiation from a backward wave oscillator (BWO) was focused on a free supersonic jet generated by a 25-μm-wide 18-mm-long pulsed slit nozzle. The spectroscopic information was collected by a hot electron InSb bolometer whose output was amplified, filtered, accumulated, and stored in the controlling computer. The typical output power fed into chamber ranged between 1 and 10 mW. The traces of the spectra were typically averaged over 500 to 4000 scans.

In the Ne · ND_3 experiment, a premixed sample of 1–2% of ammonia in neon was expanded through the 25-μm-wide, 18-mm-long slit nozzle at backing pressure of 150–155 psi. The perdeuterated ammonia was purchased from Aldrich Chemical Company (99 atom % D grade), and neon from Praxair (research grade).

In the Kr · ND_3 experiment, a mixture of 0.6–1.0% of ND_3 and 2% of krypton (AGA, 99.97% grade) in neon was expanded through the same slit nozzle at backing pressures of 80–100 psi. The experimental conditions were optimized to give the maximum signal amplitude. A rather low concentration of krypton was maintained to prevent formation of complexes with more than one krypton atom. In both cases, the beam was probed at distances 20–25 mm downstream from the nozzle.

III. THEORY

For the expressions for the energies of the VTR levels shown in Fig. 1c we used a Hamiltonian similar to that used by Schmuttenmaer *et al.* (*2, 3*):

Σ states,

$$E_{VTR}(J,\xi) = B[J(J+1)-\Omega^2] - D[J(J+1)-\Omega^2]^2 + H[J(J+1)-\Omega^2]^3 - \frac{1}{2}(-1)^{\xi}\Delta_{\Sigma}(J) \quad [3.1a]$$

Π^- states,

$$E_{VTR}(J,\xi) = B[J(J+1)-\Omega^2] - D^-[J(J+1)-\Omega^2]^2 + H[J(J+1)-\Omega^2]^3 - \left[q_{\Omega} + \frac{1}{2}(-1)^{\xi}\delta q_{\Omega}\right] \times J(J+1) + V_0 - \frac{1}{2}(-1)^{\xi}\Delta_{\Pi}(J) \quad [3.1b]$$

Π^+ states,

$$E_{VTR}(J,\xi) = B[J(J+1)-\Omega^2] - D^+[J(J+1)-\Omega^2]^2 + H[J(J+1)-\Omega^2]^3 + V_0 - \frac{1}{2}(-1)^{\xi}\Delta_{\Pi}(J) \quad [3.1c]$$

all states,

$$\Delta_{\Sigma,\Pi}(J) = \Delta^0_{\Sigma(\Pi)} - \Delta^1_{\Sigma(\Pi)}J(J+1). \quad [3.1d]$$

Here, B and D are the conventional rotational constants, common for both symmetric and antisymmetric spin states, V_0

is the energy of rotationless level of the Π state in the noninverting limit (the energy of the corresponding level in the $\Sigma 0_0$ state is equal to zero), and q_Ω is an Ω-doubling constant similar to a l-type doubling constant, which takes into account the rotational interaction of the $\Pi 1_0^-$ and $\Sigma 1_0$ states. The $\Delta_\Sigma(J)$ and $\Delta_\Pi(J)$ denote the full inversion splitting intervals in the respective Ω states, with ξ being 0 for symmetric inversion states and 1 for antisymmetric inversion states, denoted by + and − on the left hand side of Fig. 1c, respectively. The J-dependence in Eq. [3.1d] is introduced to account for the centrifugal distortion effects on the inversion splitting (*17*). The appearance of the q_Ω term uniquely in the energy expression of the Π^- state reflects the fact that this state is the one that is being pushed down by the rotational interaction while the Π^+ state remains uncoupled. The inclusion of the term δq_Ω allows for different values of the Coriolis coupling term in the different nuclear spin states. Hence, both δq_Ω and q_Ω are the effective parameters describing the net effect of the interaction of the $\Pi^- 1_0$ state with the higher excited states.

The inspection of the set of equations [3.1] shows that, apart from the inversion splitting, the energy level structure is similar to that of the diatomic molecule. The internal motion of the ammonia moiety occurs on a time scale much shorter that the overall rotation of the complex, and therefore the details of the structure of the ammonia subunit are highly averaged and allow it to be treated as a structureless pseudo atom. The inversion motion results in the splitting of the energy level structure into two separate, but similar patterns. Hence, the spectrum of the analyzed VTR band is expected to have a pattern similar to that of the spectrum of the diatomic molecule; thus, we will describe the spectral pattern as *pseudodiatomic*.

The quadrupole interaction of the nitrogen nucleus with the electric field gradient of the monomer results in the splitting of the VTR levels of the complex into sublevels with different total angular momentum $\boldsymbol{F}$ ($\boldsymbol{F} = \boldsymbol{I} + \boldsymbol{J}$). The energies $\mathcal{E}_{\mathcal{HFS}}$ of the quadrupole components, relative to the ones given in Eqs. [3.1a]–[3.1c], are provided by the following expressions (*18*):

Σ states,

$$\mathcal{E}_{\mathcal{HFS}} = -eQq_{aa} f(I, J, F) \qquad [3.2a]$$

Π states,

$$\mathcal{E}_{\mathcal{HFS}} = \left(eQq_{aa} \frac{3 - J(J+1)}{J(J+1)} \pm \frac{1}{2} eQ(q_{bb} - q_{cc}) \right) f(I, J, F). \qquad [3.2b]$$

Here $f(I, J, F)$ is the Casimir function (*17*), Q is a nuclear quadrupole moment of nitrogen atom, and the q_{ii} are the quadrupole coupling constants along the i inertial axis of the complex. It should be noted that Eqs. [3.2] result from the coupling of the total angular momentum $\boldsymbol{J}$ and the nuclear spin of the nitrogen, $\boldsymbol{I}$, to form a resulting $\boldsymbol{F}$ (*19*), whereupon the components of the electric field gradient tensor in the reference frame of the complex are expressed through those in the original, monomer-fixed reference frame, by rotating the latter through the Euler angles $(\phi, \theta, 0)$. For $\Omega = 0$, the only nonvanishing component of the field gradient tensor $\boldsymbol{q}^{(2)}$ in the new, complex-fixed coordinates, is q_0^2 which results in the only nonzero coupling constant q_{aa}. For the $\Pi^\pm$-states ($\Omega = 1$), there are also nonvanishing $\pm(q_2^{(2)} + q_{-2}^{(2)})$, where the $\pm$ sign correlates with the sign of the $\Pi^\pm$ state, which results in the last term in Eq. [3.2b]. These coupling constants are related to that of the isolated ND_3, eQq_{ND_3}, as (*3*)

$$eQq_{aa} = eQq_{ND_3} \langle P_2(\cos\theta) \rangle \qquad [3.2c]$$

$$eQq_{bb} - eQq_{cc} = eQq_{ND_3} [1 - \langle P_2(\cos\theta) \rangle], \qquad [3.2d]$$

where θ is the angle between the C_3 axis of the ammonia monomer and $\boldsymbol{R}_{vdW}$. The brackets in [3.2c] indicate the expectation value of the Legendre polynomial in the molecular state in question.

As we showed previously (*1*), the symmetric and antisymmetric inversion states correspond to different nuclear spin species transforming as A_1' and A_2', with statistical weights of 30 and 3, respectively (see Fig. 1c). The selection rules permit transitions between the states of the same nuclear spin symmetry, thus giving rise to two diatomic-like spectral patterns with components that are denoted U (upper) and L (lower) in Fig. 1, and separated by the sum of the inversion splittings in the $\Sigma 0_0$ and $\Pi 1_0$ states. To avoid confusion, we will describe components of the spectra as "upper" and "lower" implying their relative position on the frequency scale, and label corresponding states according to nuclear spin symmetry properties. The summary of the selection rules is

$$\begin{aligned} &\Psi''(\Gamma_{NS}(A_1')) \rightarrow \Psi'(\Gamma_{NS}(A_1')) \\ &\quad \text{(“upper” component, statistical weight 30)} \\ &\Psi''(\Gamma_{NS}(A_2')) \rightarrow \Psi'(\Gamma_{NS}(A_2')) \\ &\quad \text{(“lower” component, statistical weight 3)} \\ &|J'' - J'| = 0, 1 \\ &|F'' - F'| = 0, 1. \end{aligned} \qquad [3.3]$$

Hence, the transitions in the states of the different nuclear spin symmetry form two separate subbands. The inspection of the level diagram in Fig. 1c and Eqs. [3.1] show that the observed spectra only allow one to determine the sum of the Δ^0 terms in the Σ and Π states, but not the terms themselves. Assuming the inversion splittings in the two states are approximately equal, we can usefully define the average inversion splitting, Δ_I, as

$$2\Delta_I \equiv \Delta_\Sigma^0 + \Delta_\Pi^0. \qquad [3.4]$$

However, the observation of the P and R branches in the two inversion components allows for independent determination of the Δ^1 term in the upper and lower states.

IV. RESULTS

IV.1. Rotational Structure

The microwave (*4, 5, 8*) and submillimeter-wave (*8, 3*) results indicate that the NH_3 monomer undergoes almost free internal rotation in the $k = 0$ states of the argon complex. Based on that result we expect that the position of the $\Sigma 0_0 \rightarrow \Pi 1_0$ origin frequency does not depend strongly upon rare gas substitution and, in the first approximation, one should search for these transitions in the Rg · ND_3 complexes in the same region as where the Ar · ND_3 spectrum was found.

IV.1.1. Ne · ND_3

The search of the region 200–300 GHz resulted in detection of two series of transitions assigned to the $\Sigma 0_0 \rightarrow \Pi 1_0$ band of $^{20}Ne \cdot ND_3$. The spectral pattern resembles that previously reported (*1*) for Ar · ND_3 with two distinct sets of *P*, *Q*, and *R* branches, separated by roughly 3 GHz and with a relative intensity ratio of about 10, with the weaker set lying lower in frequency. These two sets of spectral lines were assigned as transitions between the nuclear spin states corresponding to the different inversion components of the complex. Additionally, another set of weak transitions has been observed in the same region, which has been assigned to the upper component of the $\Sigma 0_0 \rightarrow \Pi 1_0$ band of $^{22}Ne \cdot ND_3$. Due to the low natural abundance of the ^{22}Ne species (9.25%), only a few transitions belonging to lower component in $^{22}Ne \cdot ND_3$ were observed. Typical traces of the spectrum taken are shown on Fig. 2, and the frequencies of the measured lines are given in Tables 1, 2. In total, 64 transitions were observed in the region between 200 and 300 GHz.

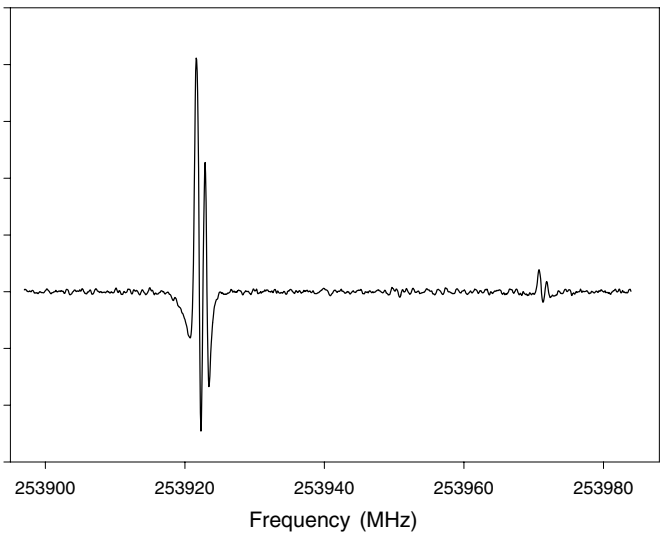

FIG. 2. An experimental trace of the Q(3) transition of $^{20}Ne \cdot ND_3$ (stronger line) at 253 921.3 MHz and Q(4) transition of $^{22}Ne \cdot ND_3$ (weaker line) at 253 970.8 MHz. The transitions occur between A_1' nuclear spin states ("upper" component). The trace is averaged over 1000 scans with an effective integration time of 500 μs.

TABLE 1
Experimentally Observed Transition Frequencies (MHz) in $^{20}Ne \cdot ND_3$ Complex

	Upper component		Lower component		
Assignment	Frequency	Δ_Q	Frequency	Δ_Q	$2\Delta_I$
P(2)	238148.5	1.13/1.56	235041.8	1.04/1.53	3106.7
P(3)	230023.3	0.90	226916.2	0.90	3106.9
P(4)	221559.3	0.98	218453.1	0.91	3106.2
P(5)	212775.9	0.91	209669.6	*n/r*	3106.3
P(6)	203695.3	0.92	—	—	—
Q(1)	253420.8	1.06/0.73	250314.1	1.0/0.70	3106.8
Q(2)	253620.4	1.17	250513.2	1.0	3107.2
Q(3)	253921.3	1.07	250812.8	1.14	3108.5
Q(4)	254322.9	1.12	—	—	—
Q(5)	254829.6	1.19	251721.1	1.21	3108.5
Q(6)	255441.2	1.12	252332.0	1.09	3109.2
Q(7)	256162.0	1.07	253052.7	1.07	3109.3
Q(8)	256995.9	1.14	253885.5	1.03	3110.4
Q(9)	257946.7	—	—	—	—
R(0)	260346.0	0.97/1.35	257239.2	1.58/1.03	3106.8
R(1)	266986.1	0.87	263879.1	0.90	3107.1
R(2)	273234.2	0.85	263879.1	0.96	3106.5
R(3)	279090.1	0.83	275983.9	0.85	3106.2
R(4)	284552.4	1.04	281446.1	0.89	3106.3
R(5)	289621.2	0.84	286515.7	*n/r*	3105.7
R(6)	294299.7	0.88	291195.4	0.58	3104.3
R(7)	298592.9	0.84	—	—	—

Note. Δ_Q is the measured quadrupole splitting (see text for details) and $2\Delta_I$ is the observed inversion separation between transitions in the upper and lower components (see Eq. [3.4]). For the lowest *J* in each branch the three quadrupole components are resolved and two splittings are reported. For higher *J*, only a single splitting is reported. The uncertainty in line positions is 0.5 MHz, and the uncertainty in measurement of the quadrupole splitting is 0.09 MHz. *n/r* indicates that due to low signal-to-noise ratio the splitting is unresolved.

The data obtained in this experiment, along with the microwave data previously reported by Wijngaarden and Jager (*16*) from the study of rotational spectra of the Ne · ND_3 in the ground $\Sigma 0_0$ state, were globally fit to the Hamiltonian Eq. [3.1]. The resulting molecular constants of Ne · ND_3 are given in the Table 3. The standard deviation of the fit is 0.45 MHz for the submillimeter-wave data, which is approximately equal to the uncertainty of experimental line measurement, and about 6 kHz for microwave data. The uncertainties of molecular parameters are one standard deviation (*16*). It should be mentioned that, unlike Ar · ND_3, the values of the centrifugal distortion constants are distinctly different for all states, particularly in $\Pi 1_0^+$ and $\Pi 1_0^-$. The $\Pi 1_0^-$ state is perturbed by a Coriolis interaction with the nearby $\Sigma 1_0$ state (*3*) while $\Pi 1_0^+$ and $\Sigma 0_0$ are not coupled with this state. The small difference in *D* in $\Pi 1_0^+$ and $\Sigma 0_0$ may be qualitatively attributed to the coupling of $\Sigma 0_0$ ($n = 0$) with the higher lying $\Sigma 0_0$ ($n = 1$) state, *n* being the van der Waals stretch quantum number (*3*).

In the case of Ne and Ar containing complexes, the amount of data derived from purely rotational transitions is insufficient to derive the sextic term *H* in the ground state of the complex. In the present experiment, we have obtained sufficient data for

TABLE 2
Experimentally Observed Transition Frequencies (MHz) in $^{22}Ne \cdot ND_3$ (Natural Abundance 9.25%)

	Upper component		Lower component		
Assignment	Frequency	Δ_Q	Frequency	Δ_Q	$2\Delta_I$
P(2)	238525.2	1.09/1.7	—	—	—
P(3)	230794.7	0.93	—	—	—
P(4)	222758.0	0.91	—	—	—
P(5)	214433.9	n/r	—	—	—
Q(1)	253112.8	1.10/0.77	250006.3	n/r	3106.4
Q(2)	253302.9	1.03	250196.1	0.94	3106.8
Q(3)	253587.5	1.14	250480.4	n/r	3107.1
Q(4)	253970.8	1.13	—	—	—
Q(5)	254451.5	1.07	—	—	—
Q(7)	255716.7	1.14	—	—	—
R(0)	259758.3	0.96/(n/r)	—	—	—
R(1)	266153.7	0.97	—	—	—
R(2)	272196.3	0.92	269090.0	0.89	3106.3
R(3)	277882.5	0.89	274776.7	0.91	3105.8
R(4)	283211.9	0.85	—	—	—
R(5)	288183.2	0.78	—	—	—
R(6)	292796.0	n/r	—	—	—
R(7)	297053.9	n/r	—	—	—

Note. The uncertainties in measurements of line positions and quadrupole splittings are 0.5 and 0.09 MHz, respectively. n/r indicates that the quadrupole structure is not resolved.

determining this parameter in both Σ and Π states and thus improving the set of parameters for the ground state.

IV.1.2. $Ar \cdot ND_3$

The experimental results on the $Ar \cdot ND_3$ complex were reported previously (*1*). A total of 46 transitions were observed in the region of 195–268 GHz. These spectral lines were assigned as transitions originating from two different inversion components corresponding to different nuclear spin states transforming as A_1' (upper component) and A_2' (lower component). In this work we have refit the data obtained in our previous work (*1*), along with microwave data obtained from measurement of the rotational transitions of the complex in the ground state, by Wijngaarden and Jager (*13*). The standard deviation of the fit is about 2 kHz for microwave, and 0.4 MHz for submillimeter-wave data. The results of the fit are summarized in Table 4. Subsequently, the structural parameters of the complex were derived from the rotational and quadrupole interaction analysis.

TABLE 3
Molecular Constants (MHz) Derived for $Ne \cdot ND_3$

Constant	Ne isotope	$\Sigma 0_0$	$\Pi^+ 1_0$	$\Pi^- 1_0$
B	20	3702.211(5)	3751.134(34)	
	22	3541.340(6)	3587.847(52)	
D	20	0.4243(4)	0.4084(11)	0.3178(13)
	22	0.3833(8)	0.3673(18)	0.2957(27)
H	20	−0.00021(1)	−0.00019(2)	
	22	−0.00023(4)	−0.00024(4)	
q_Ω	20	—	238.61(3)	
	22	—	217.19(4)	
δq_Ω	20	—	0.095(12)	
	22	—	0.120(60)	
V_0	20	255519.13(22)		
	22	255053.17(32)		
$2\Delta_I$	20	3107.09(29)		
	22	3105.74(66)		
Δ^1	20	−0.028(2)	0.020(10)	
	22	−0.028(2)	0.106(83)	

TABLE 4
Molecular Constants (MHz) Derived for $Ar \cdot ND_3$

Constant	$\Sigma 0_0$	$\Pi^+ 1_0$	$\Pi^- 1_0$
B	2600.962(1)	2618.448(8)	
D	0.0688(1)	0.0661(2)	0.0739(4)
H	$-1.43(29) \cdot 10^{-5}$	$-1.37(30) \cdot 10^{-5}$	
q_Ω	—	58.138(12)	
δq_Ω	—	0.175(8)	
V_0	234895.73(12)		
$2\Delta_I$	2872.71(19)		
Δ^1	0.0321(5)	0.0481(65)	

IV.1.3. $Kr \cdot ND_3$

A series of spectral lines attributable to the Π-bend band in $Kr \cdot ND_3$ was observed in the 195–285 GHz region which were assigned to *P*-, *Q*-, and *R*-branch transitions of the upper inversion component in the complex formed from four isotopes of krypton: ^{82}Kr (natural abundance 11%), ^{83}Kr (11%), ^{84}Kr (57%), ^{86}Kr (17%). Typical traces of the observed transitions are shown on Fig. 3. A total of 98 transitions were observed. The frequencies of the measured lines of the upper and lower inversion components for the various isotopomers are given in Tables 5 and 6, respectively. The transitions, along with the microwave spectrum of the rotational transitions of the complex in the ground state, reported by Wijngaarden and Jager (*15*), were globally fit to the energy level expression Eq. [3.1] with a resulting standard deviation of 0.4 MHz for the submillimeter-wave spectrum, and about 5 kHz for the microwave spectrum. The results of the fit are summarized in Table 7.

Unlike the neon complex, the centrifugal distortion constants in the different states are nearly identical, but still distinguishable within the quality of the fit. Since the krypton atom is much heavier than the ammonia subunit, the reduced mass asymptotically approaches the mass of the ammonia, and hence the isotope dependence of the centrifugal distortion observed is rather weak. The uncertainty of the calculation of the sextic term *H* in the

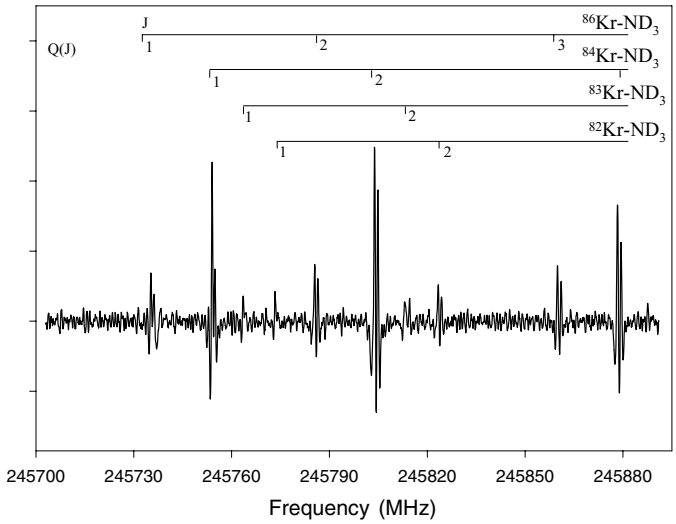

FIG. 3. An experimental trace of the beginning of a Q branch of the Kr · ND_3. Shown are $Q(1)$ and $Q(2)$ transitions of all four isotopomers of the Kr · ND_3, and $Q(3)$ of ^{86}Kr · ND_3 and ^{84}Kr · ND_3. All transitions occur between A_1' nuclear spin states. The trace is averaged over 1000 scans with an effective integration time of 500 μs.

TABLE 6
Experimentally Observed Transitions in the Lower (A_2') Component of the Most Abundant Isotopomer, ^{84}Kr · ND_3

Assignment	Frequency	Δ_Q	$2\Delta_I$
P(3)	230677.7	n/r	2654.7
P(4)	226467.9	n/r	2653.7
P(5)	222218.3	n/r	2652.7
R(1)	251128.1	1.0	2655.4
R(2)	—	—	—
R(3)	259012.6	0.94	2653.2

Note. For each transition the center of the line frequency F_e and the observed quadrupole splitting Δ_Q are given. The last column gives the individual inversion separation between the two inversion components observed for a particular transition (n/r indicates that the splitting is unresolved).

Hamiltonian Eq. [3.1] in both states in all isotopic species is of the order of the H value itself, which implies that no sextic J-dependence of the rotational energies can be observed within the experimental accuracy. Hence, this term was fixed to zero in the final fit, which left the quality of the fit essentially unchanged.

TABLE 5
Experimentally Observed Transitions in the Upper (A_1') component of Kr · ND_3

	^{82}Kr · ND_3		^{83}Kr · ND_3		^{84}Kr · ND_3		^{86}Kr · ND_3	
Assn.	Frequency	Δ_Q	Frequency	Δ_Q	Frequency	Δ_Q	Frequency	Δ_Q
P(2)	237484.9	$1.14/(n/r)$	237494.8	$1.08/(n/r)$	237504.6	1.03/1.51	237522.5	$1.07/(n/r)$
P(3)	233293.5	0.90	233313.1	0.82	233332.7	0.82	233369.7	1.01
P(4)	229062.2	0.85	229092.4	0.91	229120.7	0.80	229178.3	0.96
P(5)	224790.9	0.84	224831.7	0.84	224870.8	0.89	224948.1	0.90
P(6)	—	—	220532.2	0.90	220582.2	0.84	220680.4	0.89
P(7)	—	—	—	—	216256.6	0.84	216374.7	n/r
P(8)	—	—	—	—	211892.8	0.86		
P(9)	—	—	—	—	207491.8	0.86		
P(10)	—	—	—	—	203055.1	0.79		
P(11)	—	—	—	—	198581.7	0.85		
Q(1)	245771.7	n/r	245762.2	$(n/r)/0.83$	245752.4	1.08/0.83	245734.5	$(n/r)/0.83$
Q(2)	245821.9	0.96	245812.0	0.97	245802.6	0.99	245784.2	0.97
Q(3)	245897.7	1.0	245887.6	1.17	245877.5	1.11	245858.8	1.17
Q(4)	295998.1	1.13	245987.9	1.09	245977.9	1.13	245958.6	1.09
Q(5)	246124.4	1.16	246113.9	1.10	246103.2	1.14	246083.4	1.10
Q(6)	246275.8	1.16	246265.0	1.11	246254.5	1.16	246233.9	1.11
Q(7)	246452.9	1.23	246441.8	1.08	246430.7	1.08	246409.5	1.08
Q(8)	246654.7	1.09	246643.0	1.14	246631.5	1.13	246609.7	1.14
R(0)	249815.0	$(n/r)/0.95$	249796.2	$(n/r)/0.98$	249776.7	1.34/0.96	249742.6	$(n/r)/1.07$
R(1)	253837.3	0.76	253811.6	0.81	253783.5	0.82	253732.0	0.87
R(2)	257818.9	0.95	257782.4	0.87	257746.5	0.92	257677.7	0.86
R(3)	261754.8	0.86	261709.7	0.88	261665.8	0.90	261580.8	0.85
R(4)	265645.2	—	265592.1	—	265540.2	—	265439.8	—
R(5)	269486.0	—	269424.7	—	269365.3	—	269250.9	—
R(6)	273281.1	—	273212.3	—	273144.6	—	273014.9	—
R(7)	277024.1	—	276948.1	—	276874.1	—	276730.4	—
R(8)	—	—	—	—	280552.5	—	280395.8	—
R(9)	—	—	—	—	284178.2	—	284009.9	—

Note. For each transition the center frequency of the line and the observed quadrupole splitting Δ_Q are given in MHz. n/r indicates that the splitting is not resolved.

TABLE 7
Molecular Constants (MHz) Derived for Kr · ND_3

Constant	Kr Isotope	$\Sigma 0_0$	$\Pi^+ 1_0$	$\Pi^- 1_0$
B	82	2055.036(45)	2067.543(45)	
	83	2050.249(55)	2062.727(54)	
	84	2045.5731(6)	2058.108(22)	
	86	2036.5820(12)	2048.980(19)	
D	82	0.0342(8)	0.0337(8)	0.0370(5)
	83	0.0341(11)	0.0335(11)	0.0369(6)
	84	0.03394(1)	0.0334(3)	0.0368(1)
	86	0.03362(3)	0.0327(3)	0.0366(1)
q_Ω	82	—	33.670(22)	
	83	—	33.505(26)	
	84	—	33.348(16)	
	86	—	33.012(17)	
V_0	82		246486.5[a]	
	83		246472.1[a]	
	84		246457.48(24)	
	86		246430.9[a]	
$2\Delta_I$	82		—	
	83		—	
	84		2655.80(48)	
	86		—	
Δ^1	82	—	—	
	83	—	—	
	84	0.0431(4)	−0.101(30)	
	86	0.0428(9)	—	

Note. The sextic term H is fixed at zero value for all isotopic species. The term δq_Ω for both upper and lower states is fixed at zero value (see text for details).

[a] Since the transitions in the A_2' spin states for these isotopomers have not been observed, the origin frequency has been predicted using the transition frequency in A_1' states and the assumption that the inversion splitting does not change significantly upon isotopic substitution.

No transitions belonging to the Q branch in the less abundant nuclear spin species (A_2') are observed. At these circumstances, the Coriolis coupling constant q_Ω in the $\Pi^+ 1_0$ state cannot be determined, since it describes the splitting of the rotational levels of the $\Pi 1_0$ state into $\Pi^- 1_0$ and $\Pi^+ 1_0$, and the latter state is not experimentally observed in antisymmetric nuclear spin species, A_2' (see transitions diagram in Fig. 1c). Hence, to make the fit procedure to converge, the δq_Ω was fixed at zero, implying that the Coriolis coupling is the same in both spin states. For less abundant isotopomers, $^{82}Kr \cdot ND_3$, $^{83}Kr \cdot ND_3$, and $^{86}Kr \cdot ND_3$, no transitions in the (A_2') states were observed, hence all inversion-related terms were explicitly excluded from the fitting model by fixing them at zero values, except for $^{86}Kr \cdot ND_3$ where the microwave data (*15*) allow for determination of the centrifugal distortion effect in the inversion splitting in the ground state.

In order to avoid the competing process of formation of heavier clusters we had to keep the concentration of krypton gas as low as 2% in the mixture and restrict reservoir pressure to maximum of 100 psi. Due to these limitations, and also to the fact that krypton has several isotopes with comparable abundances, the signal-to-noise ratio was lower than in experiments with $Ne \cdot ND_3$, and therefore only a few transitions in the weaker A_2' nuclear spin states were observed. The frequencies of these transitions and corresponding individual inversion splittings are given in Table 6.

IV.2. Quadrupole Structure

As in the case of $Ar \cdot ND_3$, partially resolved quadrupole structure has been observed for $Ne \cdot ND_3$ and $Kr \cdot ND_3$ which has been fit to the hyperfine Hamiltonian, Eq. [3.2], separately from the rotation analysis. The observed rotational transitions with $J'' > 2$ are split into two components with the approximate intensity ratio 2 : 1.

The selection rules allow 6 quadrupole components for each transition in the R and P branches, and 5 components in the Q branch. With increasing J'' however, the transitions with $F' - F'' = J' - J''$ contain essentially all the transition strength and the intensities of other transitions dramatically decrease (*17*). Of the three strong transitions originating from the states with $F'' = J''$, $J'' \pm 1$, the latter two with $F'' = J'' \pm 1$ are not separated sufficiently enough to be resolved in the present experiment for $J'' > 2$, while the transition from the state with $F'' = J''$ is clearly resolved. Hence, the quadrupole structure appears as a doublet with an intensity ratio of about 2 : 1 for the two components. This experimentally measured splitting, Δ_Q, is used for the quadrupole analysis. The frequency of the weaker peak is simulated by an appropriate function of I, J, and F quantum numbers according to sets of equations [3.1], [3.2]. The frequency of the stronger peak is simulated as the center of the mass of the two transitions originating from $F'' = J'' \pm 1$ states, which are also a function of I, J, and F. Both functions contain values of eQq_{aa} and $(eQq_{bb} - eQq_{cc})$ in the upper and lower states as parameters, of which only the value of eQq_{aa} in each state is independently determined by virtue of the relationship $eQq = eQq_{aa} + eQq_{bb} - eQq_{cc}$ (Eqs. [3.2c], [3.2d]), where eQq is fixed at the value of the quadrupole coupling constant in free ammonia of −4.023 MHz (*20*). Schmuttenmaer *et al.* (*3*) showed that the value of eQq in the free and van der Waals bonded ammonia is essentially the same which indicates that the electric field gradient at the site of the nitrogen nucleus is unchanged upon complexation. Hence, the separation between the two peaks is described as a function of the three quantum numbers and two parameters, $eQq_{aa}(\Sigma 0_0)$ and $eQq_{aa}(\Pi 1_0)$, whose values can be derived from the fit of the observed quadrupole splitting Δ_Q to the described model. The value of eQq_{aa} can be related via Eqs. [3.2c], [3.2d], to the structural parameter $\langle\theta\rangle$ of the complex if one allows the substitution $\langle P_2(\cos\theta)\rangle$ by $P_2(\cos(\langle\theta\rangle))$.

It is worthwhile considering the limitations in the accuracy of the measured values of Δ_Q. Due to the signal processing and filtering, the lineshape becomes distorted and at best appears as a second derivative of the actual time-domain signal. The response function of the data acquisition hardware is fairly complex and depends on local scan rate, hence no attempts to perform signal deconvolution and to restore the original lineshape were made.

TABLE 8
Quadrupole Coupling and Structural Constants of Rg · ND_3 (Rg = Ne, Ar, Kr)

Species	van der Waals radius, A	$\Sigma 0_0$			$\Pi 1_0$		
		eQq_{aa}, MHz	$\langle\theta\rangle^d$, deg	R_{vdW}	eQq_{aa}, MHz	$\langle\theta\rangle^d$, deg	R_{vdW}
$^{20}Ne \cdot ND_3$	1.54	0.521[a]	60.20	3.692948(2)	1.002(74)	65.85(90)	3.668787(20)
$^{22}Ne \cdot ND_3$				3.688978(4)			3.664991(25)
$^{40}Ar \cdot ND_3$	1.88	0.682[b]	62.00	3.815158(1)	1.073(80)	66.78(97)	3.802398(15)
$^{82}Kr \cdot ND_3$				3.907748(40)			3.895912(60)
$^{83}Kr \cdot ND_3$	2.02	0.520[c]	60.18	3.907664(50)	1.031(74)	66.23(90)	3.895826(60)
$^{84}Kr \cdot ND_3$				3.907599(2)			3.895677(30)
$^{86}Kr \cdot ND_3$				3.907419(40)			3.895579(60)

Note. The quadrupole constants of Ar · ND_3 were refit to a one-parameter (eQq_{aa} in the Π state) model using the value of $eQq(ND_3) = -4.023$ (*20*). The values of quadrupole coupling constants in the ground state were taken from the works of Wijngaarden and Jager as indicated. The values of R_{vdW} were calculated from the observed rotational constants.

[a] Taken from a work of Wijngaarden and Jager (*16*).

[b] Taken from a work of Wijngaarden and Jager (*13*).

[c] Taken from a work of Wijngaarden and Jager (*15*).

[d] The $\langle\theta\rangle$ values are given for convenience. In the actual experiment, $\langle P_2(\cos\theta)\rangle$ is measured. See text for details.

An upper limit of the precision of the experimental measurement of the splitting has been estimated as one-half of the separation between the two transitions from states with $F'' = J'' \pm 1$, which is about 100 kHz. It is important to note that this value defines the extent of the validity of the interpretational model rather than the accuracy of the measurement of the separation of the apparent peaks, which is about 50 kHz. Hence, all fit procedures which give standard deviations smaller than 100 kHz produce results of the equal validity within the scope of this particular model. Recently, Wijngaarden and Jager have obtained fully resolved quadrupole structure of the rotational transitions of the complexes in the ground state from the microwave FT experiments (*13, 15, 16*) on all three complexes involved in the present study. The quadrupole splittings in the ground state are determined much more precisely than those from our partially resolved submillimeter-wave spectra. Hence, we have used the values of eQq_{aa} in the ground state from their work and have fit our data to the model with only one parameter, e.g., eQq_{aa} in the excited $\Pi 1_0$ state. The data presented by Wijngaarden and Jager show that the quadrupole coupling constants in the ground states of different nuclear spin and isotope species of a complex involving a particular rare gas are indistinguishable within experimental error, except the symmetric nuclear spin state of $^{22}Ne \cdot ND_3$, in which eQq_{aa} is slightly lower than for the other neon isotope. In the fitting procedure, we have used the averaged values of the quadrupole coupling constants in the ground state equal to 0.521, 0.682, and 0.520 for neon, argon, and krypton complexes, respectively. In the case of Kr · ND_3 the data obtained from the P, Q, and only part of the R branch were sufficient to produce a fit with standard deviation below the model limitations, so the splittings from the rest of the R branch of Kr · ND_3 were not included in the fit and are not reported.

The data from Ar · ND_3 obtained in the previous work (*1*) were refit to the present one parameter model discussed above, producing the corrected value of the quadrupole coupling constant in the excited state. The results of the quadrupole analysis are summarized in Table 8.

V. DISCUSSION

The experimentally obtained spectroscopic data and derived values can be analyzed from two separate perspectives. First, the rare gas substitution provides an "adjustable" molecular probe, thereby varying the strength, and possibly, the shape of the intermolecular potential surface. Second, two out of the three rare gases involved in the present study have multiple isotopes with natural abundances high enough to allow for the detection of the corresponding complexes. This gives one the opportunity to scale the kinetic part of the Hamiltonian and qualitatively study the properties of the complex with respect to mass variation while the potential surface remains essentially unchanged. In this work we will focus out attention on the rare gas dependent effects only. In the analysis of the properties of the complex depending upon rare gas substitution, we will only consider the complexes containing the most abundant isotope of the appropriate gas, namely $^{20}Ne \cdot ND_3$, $^{40}Ar \cdot ND_3$, and $^{84}Kr \cdot ND_3$.

V.1. Structural Analysis

Although the complex in question is a nonlinear polyatomic molecule, the ND_3 subunit undergoes only mildly hindered internal rotation on a time scale much shorter than the overall rotation of the complex. Hence, geometries corresponding to different orientations of the ammonia moiety are averaged over the large amplitude motion and the only structural parameter that is not thereby convoluted is the van der Waals bond distance, R_{vdW}, measured between the centers of mass of the moieties. Hence, the rotational structure is described by the simple

pseudodiatomic energy level formulae (*21*) Eq. [3.1]. The internal motion of the ammonia, however, is not completely free, and some orientations of the monomer, with respect to the complex-fixed reference frame, are more probable than others. Therefore, other structural parameters, such as the Euler angles, θ and ϕ, of the ammonia orientation in the complex-fixed frame, corresponding to the highest probability configuration, are required for a complete description of the complex. Some of this information, such as the angle θ between the C_3 axis of the ammonia and $\boldsymbol{R}_{vdW}$, which cannot be extracted from the rotational analysis, is available from the analysis of the quadrupole structure as discussed in the previous section.

For the $Ne \cdot ND_3$, $Ar \cdot ND_3$, and $Kr \cdot ND_3$ the fit, pseudodiatomic rotational constant B, yields the van der Waals bond distances in the ground $\Sigma 0_0$ state which are found to be 3.6929, 3.8152, and 3.9078 Å, respectively (see Table 8). The increase of the R_{vdW} from neon to krypton complex may be qualitatively accounted for by the increase of the effective van der Waals radius of the rare gas from 1.54 Å in neon to 2.02 Å in krypton (*22*).

Two of the rare gases involved in the study, neon and krypton, have several isotopes with natural abundances high enough to allow the detection of the corresponding complex species. The values of the R_{vdW} (Table 8) show slight dependence on the mass of the isotope, tending to increase in value from heavier to lighter isotope, which can be ascribed to the change in zero-level energy in the same potential with the variation of the reduced mass and the resulting shift of the expectation value of the radial coordinate towards smaller value with the increase of the reduced mass. The fit of the rotational structure of the $\Sigma 0_0 \rightarrow \Pi 1_0$ band in $Ar \cdot ND_3$ gives the value (*1*) of $R_{vdW} = 3.8152$ Å in the ground state, which is smaller than corresponding value for the protonated complex (*5*) $R_{vdW}(Ar \cdot NH_3) = 3.8358$ Å a change which can similarly be accounted for by the anharmonicity of the potential.

The analysis of the quadrupole structure of the transitions observed gives additional information about the orientation of the ND_3 moiety with respect to the complex-fixed axis system. It should be noted that the result for the angle θ between $\boldsymbol{R}_{vdW}$ and the C_3 axis of ammonia, derived from this analysis, is a value averaged over all possible large amplitude motions and represents only the expectation value of θ. The more correct representation of the results of quadrupole analysis is done through the expectation values of $\langle P_2(\cos\theta)\rangle$ rather than $\langle\theta\rangle$. However, the latter representation gives a more visual picture of the complex structure. The results of the structural analysis indicate (*1, 13*) that the structure of $Ar \cdot ND_3$ complex is similar to that of the protonated complex (*5*) ($R_{vdW} = 3.8358$ Å $\theta = 58.3^\circ$) with the value of $\langle\theta\rangle$ being slightly larger at 62°. Recent microwave studies indicate a similar trend in the structure of the ground state in the neon containing complex (*16*) ($R_{vdW} = 3.7227$ Å $\theta = 57.4^\circ$ for $^{20}Ne \cdot NH_3$; $R_{vdW} = 3.693$ Å $\theta = 60.2^\circ$ for $^{20}Ne \cdot ND_3$) and krypton containing complex (*15*) ($R_{vdW} = 3.922$ Å $\theta = 57.2^\circ$ for $^{84}Kr \cdot NH_3$; R_{vdW} ($Kr \cdot ND_3$) = 3.907 Å $\theta = 60.18^\circ$ for $^{84}Kr \cdot ND_3$).

The excited $\Pi 1_0$ state has been experimentally studied previously only in $Ar \cdot NH_3$ (*3*). It has been shown that with the $\Sigma 0_0 \rightarrow \Pi 1_0$ excitation the van der Waals bond in the protonated complex contracts from 3.8352 to 3.8261 Å and the value of $\langle\theta\rangle$ increases from 58.3 to 64.6 degrees. The experimental studies of this transition in the deuterated argon containing complex (*1*), as well as in the present work, show similar behavior for all $Rg \cdot ND_3$ complexes in the excited $\Pi 1_0$ state. The length of the van der Waals bond is decreased by about 0.3% in krypton and about 1% in neon containing complexes. In the excited $\Pi 1_0$ state, the values of $\langle\theta\rangle$ in all complexes increase by about 5–6 degrees compared to the $\Sigma 0_0$ state. The results are summarized in Table 8.

V.2. Inversion Splitting

An important aspect of the present work is the experimental observation of the inversion tunneling motion in the different complexes, which results in the two subbands arising from different nuclear spin species. The inversion separation defined in Eq. [3.4] results from the inversion splittings. In this work, the values of the observed separations were determined directly from the global fit of the observed frequencies of both inversion components to the Hamiltonian Eq. [3.1]. The experimental values of the derived inversion separations are given in Tables 3, 4, and 7. Van Bladel (*10, 11*) proposed a model describing the inversion splitting in the $Rg \cdot ND_3$ complexes. The Hamiltonian of the system is given by (*10*)

$$H = H_{inv}(\rho) + H_{vdW}(R, \theta, \phi, \gamma, \beta, \alpha, \rho), \qquad [5.1a]$$

where $H_{inv}(\rho)$ is the one-dimensional inversion Hamiltonian of NH_3, ρ is the inversion coordinate, and $H_{vdW}(R, \theta, \phi, \gamma, \beta, \alpha, \rho)$ describes the overall rotation of the complex and the internal motions of the two moieties with respect to each other. It is assumed that since the motion along the ρ coordinate is associated with the umbrella vibration of the monomer ($\nu_2 = 750$ cm^{-1}) and occurs on a time scale much shorter than any intermolecular motion in the complex, all ρ-dependent values in H_{vdW} can be substituted with their averages in this coordinate (*10*),

$$\begin{aligned} H_{vdW}(R, \theta, \phi, \gamma, \beta, \alpha, \rho) &= H_{vdW}(R, \theta, \phi, \gamma, \beta, \alpha, \rho_0) \\ &\equiv H_{vdW}(R, \theta, \phi, \gamma, \beta, \alpha), \end{aligned}$$

where ρ_0 is the local equilibrium value of the inversion coordinate in one of the local minima of the symmetric ammonia potential well. This means that the ρ dependence is explicitly removed from H_{vdW} and the inversion coordinate is separated from other coordinates and the Hamiltonian Eq. [5.1] takes on the form

$$H = H_{inv}(\rho) + H_{vdW}(R, \theta, \phi, \gamma, \beta, \alpha). \qquad [5.1b]$$

TABLE 9
The Effect of the Operations of PI D_{3h} Group on Rovibrational $|jk\Omega JM\rangle$ and Inversion $|\rho\rangle$ Basis Functions

Operation	Effect on basis: rovibrational	Effect on basis: inversion
E	$\|jk\Omega JM\rangle$	$\|\rho\rangle$
(123)	$\exp(2\pi ik/3)\|jk\Omega JM\rangle$	$\|\rho\rangle$
(23)*	$(-1)^{J+k}\|j-k-\Omega JM\rangle$	$\|\rho\rangle$
E*	$(-1)^{J+j+k}\|jk-\Omega JM\rangle$	$\|-\rho\rangle$
(123)*	$(-1)^{J+j+k}\exp(2\pi ik/3)\|jk-\Omega JM\rangle$	$\|-\rho\rangle$
(23)	$(-1)^{j}\|j-\mathrm{k}\Omega JM\rangle$	$\|-\rho\rangle$

The basis function set therefore, can be written as

$$\psi = |\rho\rangle|jk\Omega JM\rangle,$$

where $|\rho\rangle$ is a ground state vibrational function of a particle in free ammonia potentialsurface *localized* in one of the two minima (*10*), j is the rotational moment of ammonia monomer, k is its projection on the C_3 axis of ammonia, Ω is its projection on the van der Waals axis of the complex, and J and M are the total angular momentum of the complex and its projection on the space fixed axis. Using the projection operators to construct the symmetry adopted wavefunctions, and noting from Table 9 that only k, Ω, and ρ change their signs under the transformations of the D_{3h} group, we obtain (normalization factors are omitted)

$$\Psi^0(A_1') = |\rho\rangle[|jk\Omega\rangle + (-1)^{J+k}|j-k-\Omega\rangle] + (-1)^j|-\rho\rangle \times [|j-k\Omega\rangle + (-1)^{J+k}|jk-\Omega\rangle] \quad [5.2a]$$

$$\Psi^0(A_2'') = |\rho\rangle[|jk\Omega\rangle + (-1)^{J+k}|j-k-\Omega\rangle] - (-1)^j|-\rho\rangle \times [|j-k\Omega\rangle + (-1)^{J+k}|jk-\Omega\rangle] \quad [5.2b]$$

$$\Psi^0(A_1'') = |\rho\rangle[|jk\Omega\rangle - (-1)^{J+k}|j-k-\Omega\rangle] + (-1)^j|-\rho\rangle \times [|j-k\Omega\rangle - (-1)^{J+k}|jk-\Omega\rangle] \quad [5.2c]$$

$$\Psi^0(A_2') = |\rho\rangle[|jk\Omega\rangle - (-1)^{J+k}|j-k-\Omega\rangle] - (-1)^j|-\rho\rangle \times [|j-k\Omega\rangle - (-1)^{J+k}|jk-\Omega\rangle]. \quad [5.2d]$$

Here we have dropped from the notation quantum numbers that do not change under the transformations.

The solution to the Schrödinger equation [5.1b] has the general form

$$\Psi(\Gamma_i) = \sum C_i \Psi^0(\Gamma_i), \quad [5.3]$$

where the summation is performed over all states of the same symmetry, and Γ_i is one of the symmetry representations appearing on the left hand sides of Eqs. [5.2a]–[5.2d].

The van der Waals part of the Hamiltonian [5.1b] can be expanded (*11*) as

$$H_{vdW} = H_{rot}^m + H_{rot}^c + H_{cor} + V_{vdW}, \quad [5.4]$$

where H_{rot}^m and H_{rot}^c describe internal motion of the ammonia monomer and overall rotation of the complex, respectively, H_{cor} includes Coriolis and torsion-radial coupling terms, and V_{vdW} describes the internal molecular interaction potential which can be expanded in the spherical coordinates as (*11*)

$$V_{vdW}(R,\theta,\phi) = \sum_{l,m}(-1)^m v_{lm}(R) S_{lm}(\theta,\phi), \quad [5.5]$$

where the S_{lm} are normalized tesseral (real spherical) harmonics. The examination of the full Hamiltonian (*11*) shows that only terms off-diagonal in Ω result from H_{cor}. Schmuttenmaer *et al.* (*2*) showed that to a very good degree of approximation, Ω is a good quantum number, and for the purpose of estimation, the Coriolis, as well as the torsional-radial terms may be ignored. Hence the summation in [5.3] is performed over the states with the same J, M, and Ω and it can be rewritten as

$$\Psi(\Gamma_i) = \sum_{jk} C_{jk}^{JM\Omega} \Psi^0(\Gamma_i). \quad [5.6]$$

Since the inversion coordinate transforms according to the A_2'' representation, each J level is split into two inversion components transforming either as A_1'/A_2'' or A_1''/A_2'. These wavefunctions are given by [5.2a]/[5.2b], and [5.2c]/[5.2d], respectively. We now consider for example, a pair of functions transforming according to A_1'/A_2'' representations. Combining [5.2a], [5.2b], and [5.6], we obtain a general form for an eigenfunctions constituting this inversion pair

$$\Psi_\pm = \sum_{j,k} C_{jk}^{JM\Omega}|\rho\rangle[|jk\Omega\rangle + (-1)^{J+k}|j-k-\Omega\rangle] \pm (-1)^j|-\rho\rangle[|j-k\Omega\rangle + (-1)^{J+k}|jk-\Omega\rangle], \quad [5.7]$$

where the + sign indicates A_1' state and − sign indicates A_2'' state. The summation over k includes only ortho states, $k = 0, 3, 6\ldots$. Combining Eqs. [5.4]–[5.7] and following the argument of van Bladel *et al.* (*10*), we obtain

$$\langle\Psi_\pm|H|\Psi_\pm\rangle = E_0 + E_{vdW} \pm \frac{1}{2}\Delta_0\left[\sum_{j'k'}(-1)^{j+k} C_{j'k'}^{JM\Omega} C_{j''k''}^{JM\Omega} \delta_{j'j''}\delta_{k'k''}\right] \pm \sum_{j''j'k''k'lm}(-1)^{j'} C_{j'k'}^{JM\Omega} C_{j''k''}^{JM\Omega} \times \langle\rho|v_{lm} g_{lm}(j''j'k''k'\Omega)|-\rho\rangle, \quad [5.8a]$$

where k' and k'' run through all possible, including negative, values. The

$$E_0 = \langle \Psi_\pm | H_{inv} | \Psi_\pm \rangle = \langle \pm\rho | H_{inv} | \pm\rho \rangle$$

is the vibrational energy of the monomer. The second term,

$$E_{vdW} = \sum_{jj'kk'} C_{jk}^{JM\Omega} C_{j'k'}^{JM\Omega} \langle j'k'\Omega JM | H_{vdW} | jk\Omega JM \rangle \quad [5.8b]$$

is the energy of the van der Waals levels in the noninverting limit, and the last two sums describe the inversion tunneling interaction. The Δ_0 is the inversion splitting in the free monomer, and $g_{lm}(j''j'k''k'\Omega)$ is the Gaunt coupling coefficient (*11*). The van der Waals potential is independent of the ρ coordinate, thus Eq. [5.8a] can be rewritten as

$$\begin{aligned}\langle \Psi_\pm | H | \Psi_\pm \rangle = {} & E_0 + E_{vdW} \pm \frac{1}{2}\Delta_0 \left[\sum_{j'k'} (-1)^{j+k} \left(C_{j'k'}^{JM\Omega} \right)^2 \right] \\ & \pm \langle \rho | -\rho \rangle \sum_{j''j'k''k'lm} (-1)^{j'} \\ & \times C_{j'k'}^{JM\Omega} C_{j''k''}^{JM\Omega} v_{lm} g_{lm}(j''j'k''k'\Omega). \quad [5.8c]\end{aligned}$$

Here, $\langle \rho | -\rho \rangle$ is the overlap integral of the basis functions of the inversion coordinate localized in each of the two minima of the ammonia potential function, and v_{lm} is an expectation value of the appropriate term in [5.5] in the ground vibrational state. If the Coriolis interaction term in [5.4] is ignored, the van der Waals energy in the rotationless state ($J = 0$) is (*10*)

$$E_{vdW} = b_0 j(j+1) + \sum_{jj'kk'} C_{jk}^{JM\Omega} C_{j'k'}^{JM\Omega} \langle j'k'\Omega | V_{vdW} | jk\Omega \rangle, \quad [5.9]$$

where b_0 is the rotational constant of the monomer, and V_{vdW} is the van der Waals potential. Schmuttenmaer *et al.* has shown (*2*) that the lowest states of $Ar \cdot ND_3$ are relatively weakly mixed with the other, higher lying VTR states of the complex; therefore we can estimate contributions to both sums in [5.8c] using a perturbation theory approach.

In the absence of the van der Waals interaction described by V_{vdW}, the energies of the molecular states depend only on j and k and are equal to the energies of the states of free ammonia they correlate to. Using the first order perturbation theory we calculate the energies of the complex states, treating V_{vdW} as perturbation and calculating its diagonal elements in the basis set of symmetrized functions Eq. [5.2]. Using the expression for Gaunt coefficients g_{lm} (*11*), one obtains the expressions for the energies of the lowest van der Waals states of the complex in the noninverting limit,

$$\begin{aligned} E_{vdW}(\Sigma 0_0) &\approx \frac{1}{\sqrt{2\pi}} v_{00} \\ E_{vdW}(\Pi 1_0) &\approx 2b_0 + \frac{1}{\sqrt{2\pi}} \left[v_{00} - \frac{1}{\sqrt{5}} v_{20} \right] \quad [5.10] \\ E_{vdW}(\Sigma 1_0) &\approx 2b_0 + \frac{1}{\sqrt{2\pi}} \left[v_{00} + \frac{2}{\sqrt{5}} v_{20} \right], \end{aligned}$$

where b_0 is the rotational constant of free ammonia. Hence, the expectation value of $(1/\sqrt{2\pi})v_{00}$ is the binding energy D_0 of the complex in the ground state, and $(1/\sqrt{2\pi})v_{20}$ is approximately equal to the splitting between $\Pi 1_0$ and $\Sigma 1_0$ states. The magnitude of the latter can be estimated by taking the difference between the $j = 0 \rightarrow j = 1$ transition in the free ammonia (309.9 GHz) and the origin frequency of $\Sigma 0_0 \rightarrow \Pi 1_0$ band of $Ar \cdot ND_3$ (236.3 GHz), thus giving the estimate of $(1/\sqrt{2\pi})v_{20} = 160$ GHz ≈ 5.3 cm^{-1}, whereas the binding energy, $(1/\sqrt{2\pi})v_{00}$ of $Ar \cdot ND_3$ was found (*5, 6*) to be of the order of 100 cm^{-1}.

From Eqs. [5.8] and the discussion following Eq. [5.4] it follows that as the interaction strength approaches zero, the second sum in [5.8b] vanishes and the first summation reduces to one term, that is, wavefunctions [5.2] become the true eigenfunctions of the Hamiltonian and the van der Waals states become split by Δ_0, as in the free monomer. With the addition of the interaction potential, additional terms appear and the inversion is quenched. Using the previously obtained results Eqs. [5.8]–[5.10], we find that the inversion in the complex is equal to

$$\begin{aligned} \Delta_I &= |\langle \Psi_+ | H | \Psi_+ \rangle - \langle \Psi_- | H | \Psi_- \rangle| \\ &= \Delta_0 \left[\sum_{jk} (-1)^{j+k} \left(C_{jk}^{JM\Omega} \right)^2 \right] \\ &\quad + 2\langle \rho | -\rho \rangle \sum_{jj'kk'} C_{jk}^{JM\Omega} C_{j'k'}^{JM\Omega} \langle j'k'\Omega | V_{vdW} | jk\Omega \rangle \\ &\approx \Delta_0 \left[\sum_{jk} (-1)^{j+k} \left(C_{jk}^{JM\Omega} \right)^2 \right] + 2\langle \rho | -\rho \rangle D_0. \quad [5.11] \end{aligned}$$

Examination of the first term in Eq. [5.11] reveals that the quenching of the inversion splitting in both states results from the mixing with the states of different $j + k$ parity. Schmuttenmaer *et al.* (*2*) showed that the only significant term of this nature comes from mixing of the $\Sigma 1_0$ with the ground state, and mixing of the $\Pi 2_0$ with the $\Pi 1_0$ state. We denote the appropriate coefficient in the expansion Eq. [5.6] as $C_{j+1,k}^{JM\Omega}$ and evaluate it using the first order perturbation theory as we did in Eq. [5.10], treating van der Waals potential V_{vdW} as a perturbation. For both the $\Sigma 0_0$ and $\Pi 1_0$ states, the leading term in the expansion Eq. [5.5] which has a nonvanishing matrix element between the interacting states is v_{10}, which leads to the

expression for $C^{JM\Omega}_{j+1,k}$,

$$C^{J\Omega M}_{j+1,k} \approx \frac{1}{\sqrt{2\pi}} v_{10}(\Delta E)^{-1}, \qquad [5.12]$$

where $\Delta E = E_{\Sigma 0_0} - E_{\Sigma 1_0} \approx -2b_0$ for the $\Sigma 0_0$ state, and $\Delta E = E_{\Pi 1_0} - E_{\Pi 2_0} \approx -4b_0$ for the $\Pi 1_0$ state. For the inversion splitting *quenching*, $\delta\Delta_I \equiv (\Delta_0 - \Delta_I)$ where Δ_0 and Δ_I are the inversion splittings in the free ammonia and the complex as defined in Eq. [3.4], respectively, from [5.11] and [5.12] we obtain

$$\delta\Delta_I \approx \frac{1}{2\pi}(v_{10})^2(\Delta E)^{-2}\Delta_0. \qquad [5.13]$$

Here, for the purpose of qualitative discussion, we have ignored all odd anisotropic terms other than v_{10} resulting in the mixing of free internal rotor states with different $j+k$ parity. The numerical values of $(C^{J\Omega M}_{jk})$ for $Ar \cdot NH_3$ obtained by Schmuttenmaer *et al.* (*2*) imply that the expected inversion shifts for protonated complex are about 10% of the corresponding value in the unperturbed ammonia, which is fairly consistent with our observation of 3–15% (77–530 MHz) quenching in different complexes observed in the present study.

To calculate the contribution of the second term in [5.11], we will estimate $\langle -\rho|\rho\rangle$ by using the model inversion potential function of free ammonia employed by van Bladel *et al.* (*19*) and Millan *et al.* (*23*)

$$U(\varphi) = \frac{k}{2}\varphi^2 + a \cdot \exp[-b\varphi^2] + (V_0 - a) \qquad [5.14]$$

with parameters obtained by van Bladel *et al.* (*19*) (see Table 10). To calculate the basis wavefunctions we have used the quadratic potentials whose curvature matches that of the model potential [5.12] at its minima (dashed lines in Fig. 4). The inversion coordinate has been converted to the linear out-of-plane displacement by substitution $\rho = r_0 \cdot \sin\varphi$, where r_0 is the N–D bond length. The direct integration produced the value of $\langle -\rho|\rho\rangle \approx 3 \cdot 10^{-8}$, which results in the contribution to the inversion splitting from the last term in Eq. [5.11] being of the order

TABLE 10

Parameters of the Model Potential (*19*) Used for the Calculations of the Inversion Splittings in Rg · ND_3

Parameter	Value
k	91079.0 cm^{-1}
φ_0	0.3916 rad
a	23267.8 cm^{-1}
b	3.191 rad^{-2}
r^0_{N-D}	1.012 A
ν_0	2024.0 cm^{-1}
E	362 cm^{-1}
$k_{min}/2$	44562.85 cm^{-1}
$k_{max}/2$	−28736.61 cm^{-1}

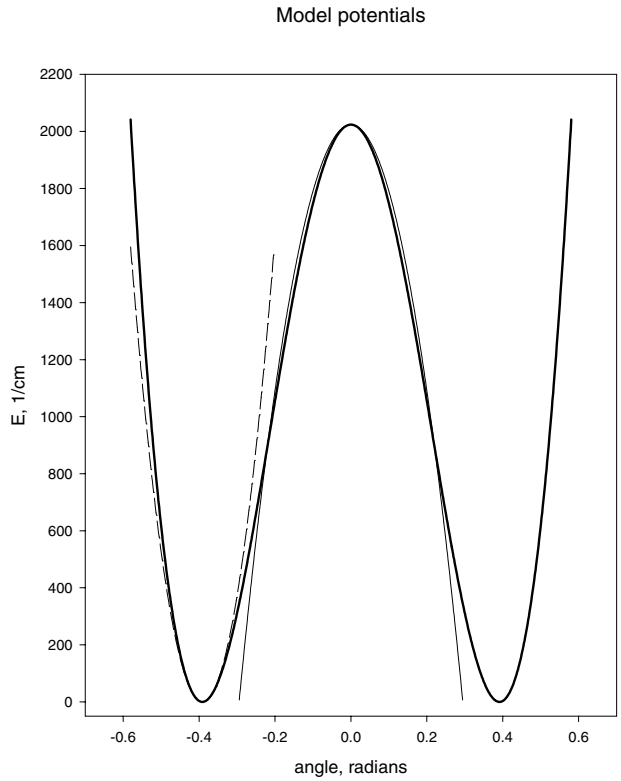

FIG. 4. The model potentials used for inversion analysis. The double-well potential plotted in thick line is a model potential used by van Bladel *et al.* (*19*); fine and dashed lines indicate the approximation harmonic potentials whose curvature matches that of th model potential at the equilibrium coordinates. The parameters of the approximation potentials are given in Table 10.

of 100 kHz. Therefore, one can ignore the last term in Eqs. [5.8], [5.11] and attribute the inversion quenching solely to the mixing between different states of a nearly free internal rotor through the anisotropic part of the intermolecular potential.

From Eq. [5.13] it follows that a quadratic dependence of the inversion quenching on the magnitude of the anisotropic term is expected. Bulski *et al.* (*7*) derived the functional form of the intermolecular potential and showed that each R-dependent term in Eq. [5.5] can be represented as a sum of the short range (SR) and long range (LR) interaction terms, i.e.,

$$v_{lm} = v^{SR}_{lm} + v^{LR}_{lm}. \qquad [5.15a]$$

The short range term decays (*7*) exponentially with R. The long range term can be expressed through a truncated series as

$$v^{LR}_{lm}(R) = -\sum_{n=6}^{10} f^{lm}_n(R) C^{lm}_n R^{-n}, \qquad [5.15b]$$

where C^{lm}_n include contribution from dispersion and induction interaction, and the damping factor $f^{lm}_n(R)$ rapidly approaches unity near the equilibrium value of the van der Waals bond length (*7*). Buckingham (*24*) and Hutson (*25*) showed that at least two leading terms, R^{-6} and R^{-7}, in both induction and dispersion terms in the long distance interaction part of the

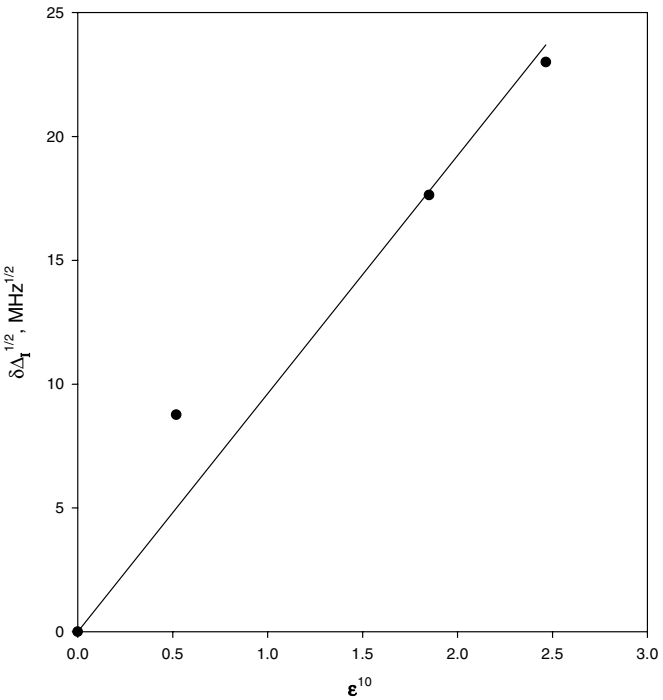

FIG. 5. Observed dependence of the inversion quenching, $\delta\Delta_I$ on the long range portion of the intermolecular potential ϵ^{10} (see text for details), in arbitrary units. The regression line was forced to pass through the origin, since the quenching vanishes for pure ND_3.

potential are proportional to the linear polarizability of the rare gas (see Eqs. (4)–(10) in Hutson's work and Eqs. (7a) and (46) in Buckingham's work).

Bulski *et al.* (*7*) showed that for v_{10}, the C_6^{10} term in Eq. [5.15b] vanishes, thus the v_{10} has a leading term of R^{-7} dependence. Hence, in the first approximation, the features of the long range part of the potential are simply scaled with linear polarizability of the rare gas α_i and the equilibrium bond distance R, and one should expect a simple quadratic dependence of the inversion quenching on $\alpha_i R^{-7}$. Figure 5 shows the plot of the square root of the inversion quenching, $(\delta\Delta_I)^{1/2}$, as a function of ϵ^{10} which is defined as a sum of the long range interaction terms in the lower and upper state of the complex, $\epsilon^{10} \equiv \alpha((R_{vdW}^{\Sigma})^{-7} + (R_{vdW}^{\Pi})^{-7})$. The experimental data for the heavier complexes are described by the quadratic dependence reasonably well, although the inversion quenching for the neon complex appears to be somewhat greater than it is expected from the simple scaling model. This deviation may possibly be accounted for by the neglect of the effect of the short range term in Eq. [5.15a], as well as the effect of the R^{-9} term in the series Eq. [5.15b] which is more important at the shorter van der Waals bond lengths.

V.3. VTR Band Origin Frequencies

One of the interesting results obtained in the study of this family of complexes is that the variation of the $\Sigma 0_0 \rightarrow \Pi 1_0$ origin frequencies does not follow a pattern comparable to that observed in other complexes. For example, in the Rg · CO family of complexes, which feature a T-shape configuration, the origin frequency of the corresponding transition monotonically increases from Xe · CO to Ne · CO (*26–28*). However, in the family of the ammonia–rare gas complexes, the origin frequency reaches its minimum at $Ar \cdot ND_3$.

The inspection of the approximate expression for the energies of the VTR states, Eq. [5.10], indicates that the origin frequency in the first order approximation should be a function of the term v_{20}. The detailed calculation of the origin frequency requires the knowledge of the potential function and the energy structure of the complex, information that cannot be extracted from the available experimental data. Therefore, in the discussion below we simply try to rationalize the obtained results from a qualitative analysis.

In Eq. [5.10] the terms arising from the interaction potential have the general form of a sum on the right hand side of Eq. [5.9]. The direct substitution of the expression Eq. [5.5] into Eq. [5.9] leads to

$$E_{vdW} = b_0 j(j+1) + \sum_{jj'kk'lm} C_{jk}^{JM\Omega} C_{j'k'}^{JM\Omega} \times \langle j'k'\Omega|(-1)^m v_{lm}(R) S_{lm}(\theta,\phi)|jk\Omega\rangle. \quad [5.16]$$

Assuming only the $m = 0$ terms dominate (*2*), and noting that $S_{l0}(\theta,\phi) = Y_m^l(\theta,\phi) = (\frac{2l+1}{4\pi})^{1/2} P_l(\cos\theta)$, we rewrite Eq. [5.16] as

$$E_{vdW} = b_0 j(j+1) + \sum_{jj'kk'l} v_{l0} C_{jk}^{JM\Omega} C_{j'k'}^{JM\Omega} \times \left(\frac{2l+1}{4\pi}\right)^{1/2} \langle j'k'\Omega|P_l(\cos\theta)|jk\Omega\rangle. \quad [5.17]$$

The v_{lm} term has the same meaning as in Eq. [5.8b]. Here, we also neglected the torsional-radial coupling, thus assuming that values of v_{lm} are the same in both ground and excited states. The matrix element, along with the normalization factor in front, is the Gaunt coupling coefficient g_{l0} (*11*),

$$E_{vdW} = b_0 j(j+1) + \sum_{jj'kk'l} v_{l0} C_{jk}^{JM\Omega} C_{j'k'}^{JM\Omega} g_{l0}(j, j', k, k', \Omega). \quad [5.18]$$

On the other hand, Eq. [5.17] can be rewritten as

$$E_{vdW} = b_0 j(j+1) + \sum_l v_{l0} \left(\frac{2l+1}{4\pi}\right)^{1/2} \left[\sum_{j'k'} C_{j'k'}^{JM\Omega} \langle j'k'\Omega|\right] \times |P_l(\cos\theta)| \left[\sum_{jk} C_{jk}^{JM\Omega}|jk\Omega\rangle\right] = b_0 j(j+1) + \sum_l v_{l0} \left(\frac{2l+1}{4\pi}\right)^{1/2} \langle P_l(\cos\theta)\rangle, \quad [5.19]$$

where $\langle P_l(\cos\theta)\rangle$ is the expectation value of a function in the molecular state, in the same sense as it has been discussed in Section 4.2. The origin frequency of the VTR band in the manifold correlating to $j''=0, k''=0 \rightarrow j'=1, k'=0$ is thus given by

$$\nu = 2b_0 + \sum_l v_{l0}\left(\frac{2l+1}{4\pi}\right)^{1/2}[\langle\Psi'|P_l(\cos\theta)|\Psi'\rangle - \langle\Psi''|P_l(\cos\theta)|\Psi''\rangle], \quad [5.20]$$

where Ψ', Ψ'' are the functions of the general form of Eq. [5.6], and the two terms in square brackets in Eq. [5.20] expand as shown in Eqs. [5.18], [5.19]. Equations [5.17]–[5.20] show that the energy of the complex states, as well as the transition frequency, is not simply scaled with values of an anisotropic terms v_{l0} $(l \neq 0)$ in the potential function, but also depends on the mixing between states and the resulting change of the orientation of the monomer in the complex-fixed reference frame. Indeed, in the limit of the unmixed states, for example, $\langle j=0, k=0, \Omega=0|P_l(\cos\theta)|j=0, k=0, \Omega=0\rangle = 0$ for all nonzero l and therefore in this limit, the averaged monomer orientation is independent of the details of van der Waals potential.

The experimental data are sufficient to only determine one significant coupling term in Eq. [5.17], and therefore, only one coefficient in the sum in Eq. [5.19]. The quadrupole analysis indicates that at least one of the terms, $\langle P_2(\cos\theta)\rangle$, does have an anomalously large value in the ground state of the Ar · ND_3 complex, which also exhibits an unexpectedly low value of the origin frequency. However, the accurate modeling of the origin frequencies of the VTR bands requires more experimental data and extends beyond the scope of the present paper.

VI. CONCLUDING REMARKS

The rotational structure corresponding to the hindered rotation bands in three complexes, Ne · ND_3, Ar · ND_3, and Kr · ND_3 has been observed and analyzed. The origin frequencies of these complexes all lie fairly close to the frequency of the corresponding rotational transition ($j=0, k=0 \rightarrow j=1, k=0$) in the free ND_3, which provides experimental evidence for nearly free internal rotation of the ND_3 moiety in the complex, only weakly hindered by the anisotropic parts of the PES of the complex. The rotational and quadrupole analysis indicate that all three complexes studied in this and a previous (*1*) paper have very similar structure in their lowest states correlating with $k=0$ states of the free ammonia. The analysis of the experimentally observed values of the inversion splitting, combined with the analysis of the origin frequencies and quadrupole structure of the $\Sigma 0_0 \rightarrow \Pi 1_0$ bands allows one to rationalize the apparent anomaly in the dependence of the origin frequencies with the rare gas substitution. An approximate quadratic dependence of the inversion quenching on van der Waals interaction strength is experimentally found and qualitatively explained using a perturbation theory analysis.

ACKNOWLEDGMENTS

We thank Mykola Bataiev for help with the experiments. We also thank the National Science Foundation for support of this work (Grants CHE-9974404 and CHE-0077974).

REFERENCES

1. D. G. Melnik, S. Gopalakrishnan, T. A. Miller, S. P. Belov, and F. C. DeLucia, *J. Chem. Phys.* **114,** 6100 (2001).
2. C. A. Schmuttenmaer, R. C. Cohen, and R. J. Saykally, *J. Chem. Phys.* **101,** 146 (1994).
3. C. A. Schmuttenmaer, R. C. Cohen, J. G. Loeser, and R. J. Saykally, *J. Chem. Phys.* **95,** 9 (1991).
4. G. T. Fraser, D. D. Nelson, A. Charo, and W. Klemperer, *J. Chem. Phys.* **82,** 2535 (1985).
5. D. D. Nelson, Jr., G. T. Fraser, K. Zhao, F. J. Lovas, R. D. Suenram, and W. Klemperer, *J. Chem. Phys.* **85,** 5512 (1986).
6. G. Chalasinski, S. M. Cybulski, M. M. Szczesniak, and S. Scheiner, *J. Chem. Phys.* **91,** 7809 (1989).
7. M. Bulski, P. E. S. Wormer, and A. van der Avoird, *J. Chem. Phys.* **94,** 491 (1991).
8. E. Zwart, H. Linnartz, W. L. Meerts, G. T. Fraser, D. D. Nelson, and W. Klemperer, *J. Chem. Phys.* **95,** 793 (1991).
9. D.-H. Gwo, M. Havenith, K. L. Busarow, R. C. Cohen, C. A. Schmuttenmaer, and R. J. Saykally, *Mol. Phys.* **71,** 453 (1990).
10. J. W. I. van Bladel, A. van der Avoird, and P. E. S. Wormer, *J. Phys. Chem.* **95,** 5414 (1991).
11. J. W. I. van Bladel, A. van der Avoird, and P. E. S. Wormer, *J. Chem. Phys.* **94,** 501 (1991).
12. C. A. Schmuttenmaer, J. G. Loeser, and R. J. Saykally, *J. Chem. Phys.* **101,** 139 (1994).
13. J. van Wijngaarden and W. Jager, *J. Chem. Phys.* **114,** 3968 (2001).
14. A. Grushow, W. A. Burns, S. W. Reeve, M. A. Dvorak, and K. R. Leopold, *J. Chem. Phys.* **100,** 2413 (1994).
15. J. van Wijngaarden and W. Jager, *Mol. Phys.* **99,** 1215 (2001).
16. J. van Wijngaarden and W. Jager, *J. Chem. Phys.* **115,** 6504 (2001).
17. C. H. Townes and A. L. Schawlow, "Microowave Spectroscopy." McGraw–Hill, New York, 1955.
18. E. Zwart and W. L. Meerts, *Chem. Phys.* **151,** 407 (1991).
19. J. W. I. van Bladel, A. van der Avoird, and P. E. S. Wormer, *Chem. Phys.* **165,** 47 (1992).
20. A. S. Bashkin, *USSR Opt. Spektrosk.* **27,** 360 (1969).
21. Y. Xu and A. R. W. McKellar, *Mol. Phys.* **88,** 859 (1996).
22. A. I. Kitaigorodsky, "Molecular Crystals and Molecules." Academic Press, New York, 1973.
23. J. Millan, N. Halberstat, G. van der Sanden, and A. van der Avoird, *J. Chem. Phys.* **106,** 9141 (1997).
24. A. D. Buckingham, *Adv. Chem. Phys.* **12,** 107 (1967).
25. J. M. Hutson, *J. Chem. Phys.* **91,** 4448 (1989).
26. M. Hepp, W. Jager, I. Pak, and G. Winnewisser, *J. Mol. Spectrosc.* **176,** 58 (1996).
27. G. Winnewisser, B. S. Dumesh, I. Pak, L. A. Surin, F. Lewen, D. A. Roth, and F. S. Rusin, *J. Mol. Spectrosc.* **192,** 243 (1998).
28. K. A. Walker and A. R. W. McKellar, *J. Mol. Spectrosc.* **205,** 331 (2001).